PERGAMON

International Journal of Solids and Structures 38 (2001) 2171–2187

INTERNATIONAL JOURNAL OF SOLIDS and STRUCTURES

www.elsevier.com/locate/ijsolstr

Micromechanics characterization of constraint and ductile tearing effects in small scale yielding fracture

Euclydes Trovato Neto, Claudio Ruggieri *

Department of Naval Architecture and Ocean Engineering, Av. Prof. Mello Moraes, 2231 (PNV-EPUSP), São Paulo, SP 05508-900, Brazil

Received 27 August 1999; in revised form 10 February 2000

Abstract

This study describes a methodology based on a local failure model to predict the strong effects of constraint variations on (macroscopic) cleavage fracture toughness. We limit our focus to a stress-controlled, cleavage mechanism for material failure and adopt the Weibull stress (σ_w) as the local parameter to describe crack-tip conditions. A central feature of the present investigation involves the interpretation of σ_w as a *macroscopic* crack driving force and the implications of its use in assessments of brittle fracture behavior. When implemented in a finite element code, the computational model predicts the evolution of Weibull stress with crack-tip stress triaxiality and stable crack growth. The small-scale yielding analyses under varying levels of T-stress exhibit the essential features of the micromechanics approach in correlating macroscopic fracture toughness with constraint variations and ductile tearing.

Keywords: Cleavage fracture; Constraint; Ductile tearing; Statistical effects; Local approach; Weibull stress

1. Introduction

Conventional fracture mechanics methodologies to assess unstable cracking behavior (cleavage fracture) of different cracked bodies (i.e., laboratory specimens and engineering structures) rely on the similarity of their respective crack-tip stress and deformation fields. Under small scale yielding (SSY) conditions, a single parameter, such as the linear elastic stress intensity factor, K, and the J-integral (or, equivalently, the crack-tip opening displacement, CTOD or δ), uniquely scales the elastic–plastic near-tip fields. In the present context, SSY is meant to pertain to loading conditions for which near-tip plasticity is well contained and controlled by the elastic fields for an infinite crack. To the extent that such one-parameter singular fields dominate over microstructurally significant size scales (i.e., the fracture process zone (FPZ) of a few CTODs ahead of a macroscopic crack), the parameters K and J (δ) fully describe the local conditions leading to unstable (cleavage) failure (see, e.g., the review by Hutchinson, 1983).

* Corresponding author. Fax: +55-11-818-5717.
E-mail address: cruggi@usp.br (C. Ruggieri).

0020-7683/01/$ - see front matter
PII: S0020-7683(00)00160-8

However, fracture testing of ferritic structural steels in the ductile-to-brittle (DBT) transition region consistently reveals a significant effect of specimen geometry and loading mode (bending vs. tension) in cleavage toughness values as measured by the critical parameters K_{Ic}, J_c or δ_c, (see Sorem et al., 1991; De Castro et al., 1979 for illustrative data). These studies show significant elevations in the elastic–plastic fracture toughness for shallow crack SE(*B*) specimens and tension geometries of ferritic steels tested in the transition region, where transgranular cleavage triggers macroscopic fracture. At increased loads in a finite body, such as a cracked specimen or structure, the initially strong SSY fields gradually change to fields under large scale yielding (LSY) as crack-tip plastic zones increasingly merge with the global bending plasticity on the nearby traction free boundaries. This phenomenon, often termed *loss of constraint*, contributes to the *apparent* increased toughness of shallow cracked and tension loaded geometries observed in fracture testing. Once SSY conditions no longer apply, larger *J*-values in the finite body are necessary to generate a highly stressed region ahead of crack tip sufficient to trigger cleavage. These features have enormous practical implications in defect assessment procedures, particularly repair decisions and life extension programs of in-service structures as well as structural design specifications.

These limitations of single parameter fracture mechanics approaches to characterize the fracture behavior of fully yielded crack geometries motivated the development of micromechanics models based upon a probabilistic interpretation of the fracture process (most often referred to as *local approaches*). Attention has been primarily focused on probabilistic models incorporating weakest link statistics to describe material failure caused by stress-controlled transgranular cleavage. By coupling macroscopic measures of fracture toughness (*J*, CTOD) with micromechanics models for material failure ahead of the crack tip, researchers endeavour to *predict*, rather than correlate, constraint effects on fracture toughness. The seminal work of Beremin (1983) provides the basis for establishing a relationship between the microregime of fracture and macroscopic crack driving forces (such as the *J*-integral) by introducing the Weibull stress (σ_w) as a probabilistic fracture parameter. Retaining contact with conventional approaches, this fracture parameter conveniently characterizes macroscopic fracture behavior for a wide range of loading conditions and crack configurations.

The central feature in the above methodologies adopts the simple axiom that unstable crack propagation (cleavage) occurs at a critical value of the Weibull stress; under increased remote loading (as measured by J), differences in evolution of the Weibull stress reflect the potentially strong variations of near-tip stress fields. This also permits a convenient treatment of ductile tearing effects on macroscopic fracture toughness. For materials having sufficient resistance to cleavage fracture in the mid transition region, intense plastic strains coupled with high stresses directly ahead of the blunting crack tip generally produce ductile tearing prior to unstable crack propagation by cleavage. This "competition" between local failure by cleavage and ductile mechanisms controls the cleavage fracture resistance of ferritic steels in the DBT regime. Ductile extension of the crack front alters the stress histories (relative to a stationary crack) in the material ahead of the blunting region and increases the volume of the FPZ (Varias and Shih, 1993; Dodds et al., 1993). Since evaluation of the Weibull stress occurs over a relevant (volume) of near-tip material termed the process zone, this approach reflects ductile crack growth effects on the local stress–strain fields that drive the microscale fracture. The Weibull stress then describes *both* the effects of stressed volume and the potentially strong changes in the character of the near-tip stress fields due to constraint loss and ductile crack extension.

The plan of the paper is as follows. In the next section, we present an overview of local (micromechanics) modeling of cleavage fracture incorporating statistics of microcracks. The approach builds upon weakest link theory and introduces the Weibull stress (σ_w) as a probabilistic fracture parameter. Numerical methods and geometric models applicable for SSY analyses are then described with emphasis on realistic modeling of ductile crack growth using the computational cell methodology. A simplified form of the Gurson–Tvergaard (GT) (Gurson; Tvergaard, 1990) constitutive model for dilatant plasticity serves to predict microscopic void growth within a layer of cells defined over the crack plane. Our SSY analyses provide key

results for stationary and growing cracks to assess effects of constraint and ductile tearing on cleavage fracture using a local fracture parameter. The paper also explores development of a toughness scaling methodology based upon Weibull stress trajectories for different constraint conditions which enables assessment of constraint loss in conventional fracture specimens. The present study builds upon previous work based on a local approach for fracture by Ruggieri and Dodds (1996a) and extends their analyses to cover a wider range of parametric values and materials options. Both works, when taken together, provide a fairly extensive body of results against which the robustness of the local fracture parameter (σ_w) can be weighed.

2. Local modeling of cleavage fracture incorporating statistics

2.1. Probabilistic fracture parameter: the Weibull stress

Limiting attention to the specific micromechanism of transgranular cleavage, we consider an arbitrarily stressed body where a macroscopic crack lies in a material containing randomly distributed flaws as illustrated in Fig. 1. FPZ ahead of the crack tip is defined as the highly stressed region where the local operative mechanism for cleavage takes place; this region contains the potential sites for cleavage cracking. For the purpose of developing a probabilistic model for brittle fracture, we divide the FPZ ahead of crack tip in a large number of *unit* volumes statistically independent; each unit volume contains a substantially number of statistically independent microflaws uniformly distributed.

The statistical nature of brittle fracture underlies a simplified treatment for unstable crack propagation of the configuration represented in Fig. 1(a). Based upon probability theory and invoking the Poisson postulates (see, e.g., Feller, 1957), the elemental failure probability, $\delta\mathscr{P}$, is related to the distribution of the largest flaw in a reference volume of the material, which can be expressed as

$$\delta\mathscr{P} = \delta V \int_{a_c}^{\infty} g(a)\,\mathrm{d}a \tag{1}$$

where $g(a)\,\mathrm{d}a$ defines the average number of microcracks per unit volume having sizes between a and $a + \mathrm{d}a$. Here, a common assumption adopts an asymptotic distribution for the microcrack density in the form $g(a) = (1/V_0)(r_0/a)^r$, where r and r_0 are parameters of the distribution and V_0 denotes a reference volume (Freudenthal, 1968; Evans and Langdon, 1976). The implicit distribution of fracture stress can be

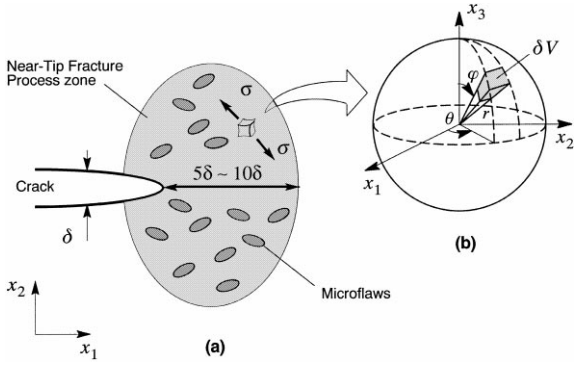

Fig. 1. (a) FPZ ahead a macroscopic crack containing randomly distributed flaws; (b) unit volume ahead of crack tip subjected to a multiaxial stress state.

made explicit by introducing the dependence between the critical microcrack size, a_c, and stress in the form $a_c = (K^2/Y\sigma^2)$, where Y represents the specimen dependent geometry factor and σ denotes a tensile (opening) stress acting on the microcrack plane. A simple manipulation of this expression on the basis of weakest link statistics provides the basis for establishing a relationship between the microregime of fracture and macroscopic crack driving forces (such as the J-integral) for the fracture stress of a cracked solid as (Beremin, 1983; Ruggieri and Dodds, 1996a, b; 1997; 1998)

$$F(\sigma_1) = 1 - \exp\left[-\frac{1}{V_0} \int_{\Omega} \left(\frac{\sigma_1}{\sigma_u} \right)^m \mathrm{d}\Omega \right], \tag{2}$$

where Ω denotes the volume of the (near-tip) FPZ, V_0 is a reference volume and σ_1 is the maximum principal stress acting on material points inside the FPZ. Ruggieri and Dodds (1996a, b; 1997, 1998) define the FPZ as the loci $\sigma_1 \geqslant \lambda\sigma_0$, with $\lambda \approx 2$. Alternative definitions for the FPZ include the plastic region ahead of the macroscopic crack $\sigma_e \geqslant \sigma_0$ where σ_e denotes the equivalent Mises stress (Beremin, 1983; Mudry, 1987).

Following Beremin (1983), the Weibull stress is defined as the stress integral

$$\sigma_w = \left[\frac{1}{V_0} \int_{\Omega} \sigma_1^m \mathrm{d}\Omega \right]^{1/m}. \tag{3}$$

which permits rewriting the stress integral of Eq. (2) in the form

$$F(\sigma_w) = 1 - \exp\left[-\left(\frac{\sigma_w}{\sigma_u} \right)^m \right]. \tag{4}$$

This expression defines a two-parameter Weibull distribution (Weibull, 1939) for the random variable σ_w. Parameters m and σ_u appearing in Eq. (4) denote the Weibull modulus and the scale parameter of the Weibull distribution.

2.2. Generalization of the Weibull stress for a growing crack

The Weibull stress describes local conditions leading to unstable (cleavage) failure and appears, at least as a first approximation, to remain applicable during small amounts of ductile crack extension. Highly localized, non-planar crack extension and void growth at the larger inclusions, both of which occur over a scale of $\lesssim \delta_{Ic}$ (the CTOD at *onset* of crack growth initiation), should not alter the material properties m and σ_u over the much larger process zone relevant for cleavage initiation. Further, small amounts of ductile crack growth modify the stress history of material points within the process zone for cleavage fracture which affects directly the evolution of Weibull stress. A detailed discussion of the approach adopted here for generating the evolution of the Weibull stress with J (or equivalently CTOD) for a growing crack is given by Ruggieri and Dodds (1996a).

Fig. 2 illustrates the development of the *active* FPZ (recall that the FPZ is defined as the loci where $\sigma_1 \geqslant \lambda\sigma_0$ with $\lambda \approx 2$) given by a snapshot of the stress field ahead of the growing crack. Points on such a contour all lie within the forward sector $|\theta| \leqslant \pi/2$. The envelope of all material points for which $\sigma_1 \geqslant \lambda\sigma_0$ during the history of growth defines an alternative, *cumulative* process zone. Consequently, the 3-D form of the Weibull stress for a growing crack becomes simply

$$\sigma_w = \left[\frac{1}{V_0} \int_{\Omega^*} \sigma_1^m \mathrm{d}\Omega^* \right]^{1/m}, \tag{5}$$

where Ω^* denotes the active volume of the FPZ, $\sigma_1 \geqslant \lambda\sigma_0$, which moves forward with the advancing tip. The proposed generalization of σ_w to include ductile tearing maintains the relative simplicity of computa-

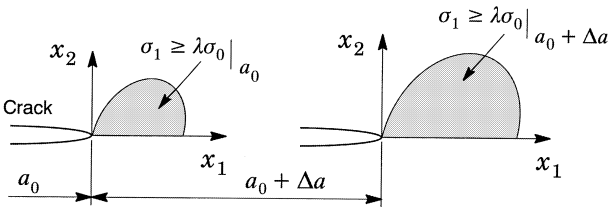

Fig. 2. Schematic representation for the evolution of the FPZ for a growing crack. The crack has advanced from $a = a_0$ to $a = a_0 + \Delta a$.

tions while, at the same time, fully incorporating the effects of alterations in the stress field ahead of the crack tip.

3. Computational procedures and geometric models

3.1. Overview of crack growth modeling using computational cells

The computational cell methodology proposed by Xia and Shih (1995a) (Xia et al., 1995b) provides a model for ductile crack extension that includes a realistic void growth mechanism, and a microstructural length-scale physically coupled to the size of the FPZ. Void growth remains confined to a layer of material symmetrically located about the crack plane, as illustrated in Fig. 3(a), and having thickness D, where D is associated with the mean spacing of the larger, void initiating inclusions. This layer consists of cubical cell elements with dimension D on each side; each cell contains a cavity of initial volume fraction f_0 (the initial void volume divided by cell volume). As a further simplification, the void nucleates from an inclusion of relative size f_0 immediately upon loading. Progressive void growth and subsequent macroscopic material softening in each cell are described with the Gurson–Tvergaard (GT) constitutive model for dilatant plasticity (Gurson, 1977; Tvergaard, 1990). Fig. 3(b) shows the typical, plane strain finite element representation of the computational cell model where symmetry about the crack plane requires elements of size $D/2$. Material outside the computational cells, the "background" material, follows a conventional J_2 flow theory of plasticity and remains undamaged by void growth in the cells.

When f in the cell incident on the current crack tip reaches a critical value, f_E (which typically has a value of 0.15–0.25), the computational procedure removes the cell thereby advancing the crack tip in discrete increments of the cell size. The final stage of void linkup with the macroscopic crack front occurs by reducing the remaining stresses to zero in a prescribed manner. Tvergaard (1990) refers to this process as the element extinction or vanish technique. This cell extinction process creates new traction free surfaces in a controlled manner and also eliminates numerical difficulties in the finite strain computations. Ruggieri and Dodds (1996c) provide further details of the computational implementation of the cell extinction scheme used in the present numerical analyses.

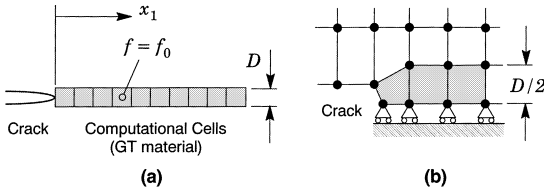

Fig. 3. Modeling of ductile tearing using computational cells.

Material properties required for this methodology include: for the background material Young's modulus (E), Poisson's ratio (v), yield stress (σ_0) and hardening exponent (n) or the actual measured stress–strain curve; and for the computational cells: D and f_0 (and of much less significance f_E). The background material and the matrix material of the cells generally have identical flow properties. Using an experimental J-Δa curve obtained from a conventional SE(B) or $C(T)$ specimen, a series of finite element analyses of the specimen are conducted to calibrate values for the cell parameters D and f_0 which bring the predicted J-Δa curve into agreement with experiment. Experience with plane–strain finite element analyses of SE(B) and $C(T)$ specimens to estimate D and f_0 for common structural and pressure vessel steels suggests values of 50–200 μm for D, 0.001–0.005 for f_0, with f_E typically 0.15–0.20. Once determined in this manner using a specific experimental R-curve, D and f_0 become "material" parameters and remain fixed in analyses of all other specimen geometries for the same material.

3.2. Finite element models

The modified boundary layer (MBL) model (Larsson and Carlsson, 1973; Rice, 1974) simplifies the generation of numerical solutions for stationary and growing cracks under well-defined SSY conditions with varying levels of constraint. Fig. 4 shows the plane–strain finite element model for an infinite domain, single-ended crack problem; Mode I loading of the far field permits analysis using one-half of the domain as shown. With the plastic region limited to a small fraction of the domain radius, $R_p < R/20$, the general form of the asymptotic crack-tip stress fields well outside the plastic region is given by Williams (1957)

$$\sigma_{ij} = \frac{K_I}{\sqrt{2\pi r}} f_{ij}(\theta) + T\delta_{1i}\delta_{1j}, \tag{6}$$

where K is the stress intensity factor, $f_{ij}(\theta)$ define the angular variations of in-plane stress components, and the non-singular term T represents a tension (or compression) stress parallel to the crack. Numerical solutions for different levels of T/σ_0 are generated by imposing displacements of the elastic, Mode I singular field on the outer circular boundary ($r = R$) which encloses the crack

$$u(R,\theta) = K_I \frac{1+v}{E}\sqrt{\frac{R}{2\pi}}\cos\left(\frac{\theta}{2}\right)(3-4v-\cos\theta) + T\frac{1-v^2}{E}R\cos\theta, \tag{7}$$

$$v(R,\theta) = K_I \frac{1+v}{E}\sqrt{\frac{R}{2\pi}}\sin\left(\frac{\theta}{2}\right)(3-4v-\cos\theta) + T\frac{v(1+v)}{E}R\sin\theta. \tag{8}$$

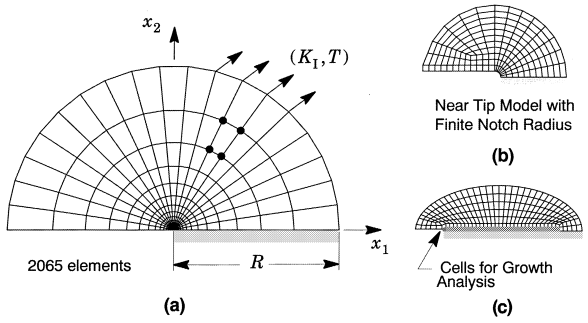

Fig. 4. SSY model with (K, T) fields imposed on boundary.

Stationary crack analyses employ a conventional mesh configuration having a focused ring of elements surrounding the crack front with a small key-hole at the crack tip; the radius of the key-hole, ϱ_0, is 2.5 μm (0.0025 mm) with $R/D = 10^6$. This SSY model has one thickness layer of 2065 8-node, 3-D elements with plane–strain constraints imposed ($w = 0$) on the nodes. Evaluation of the Weibull stress requires integration over the process zone, including the region as $r \to 0$. For crack growth analyses, the model has a single layer of 120 computational cells along the crack plane, with the plastic behavior of each cell as described in Section 3.1. These computational cells have a fixed size of $D/2 \times D/2$, with $D = 200$ μm and $R/D = 112\,500$. Fig. 3(b) shows the initial crack-tip geometry for the growth analyses.

The SSY model has a small initial root radius at the crack front (blunt tip) which provides two numerical benefits: (1) it accelerates convergence of the finite–strain plasticity algorithms during the initial stage of blunting, and (2) it minimizes numerical problems during computation of the Weibull stress over material incident on the crack tip. To limit effects of the initial root radius on Weibull stress calculations, the CTOD (δ) is required to equal four times the initial radius (ρ_0) at a deformation consistent with $\sigma_0 b/J = 250$, where σ_0 is the reference yield stress (see Section 3.3) and b is the remaining crack ligament. This condition requires $\rho_0 \approx 2.5$ μm for SSY model and flow properties considered in this work. A series of SSY analyses containing a range of initial root radii confirm that the Weibull stress trajectories after reaching steady state conditions become independent of the initial root radius for $\delta/\rho_0 > 4$. However, prior to reaching steady state conditions, the initial root radius does affect the Weibull stress as the near-tip stress fields are depedent upon the blunt tip radius and local geometries (such as, for example, mesh details). We do not consider this an important issue in the present study since the load levels prior to reaching steady state conditions are very small and are not very relevant in fracture mechanics analyses for the material properties considered in the present work. For example, cleavage fracture toughness levels for typical structural steels under essentially SSY conditions may range from 60 to 150 MPa $\sqrt{\text{m}}$; such values are already within the steady state region (therefore independent of the initial root radius) for the MBL model employed.

Section 6 outlines a toughness scaling methodology based upon the Weibull stress to assess effects of constraint loss in conventional fracture specimens. The numerical solutions employ the SSY model described above and 3-D finite element analyses for a plane-side deep notch ($a/W = 0.5$) SE(B) specimen with $B = 25$ mm [1(T)] and conventional geometry ($W/B = 2$). Here, a denotes the crack length and W is the specimen width. To maintain consistency with the finite element models for the SSY analyses, the SE(B) specimen has similar level of mesh refinement at the crack tip as the SSY model for stationary crack. The quarter-symmetric, 3-D models for the SE(B) specimen has 18500 nodes and 16 000 elements with 14 variable thickness layers defined over the half-thickness ($B/2$); the thickest layer is defined at centerplane ($x_3 = 0$) with thinner layers defined near the free surface ($x_3 = B/2$) to accommodate strong thickness variations in the stress distribution.

3.3. Constitutive models

To describe the evolution of void growth and associated macroscopic material softening in the computational cells, we adopt the Gurson (1977) and Tvergaard (1990) potential function (g) for plastic flow in porous media

$$g(\sigma_e, \sigma_m, \overline{\sigma}, f) = \left(\frac{\sigma_e}{\overline{\sigma}}\right)^2 + 2q_1 f \cosh\left(\frac{3q_2\sigma_m}{2\overline{\sigma}}\right) - \left(1 + q_3 f^2\right) = 0, \tag{9}$$

where σ_e denotes the effective Mises (macroscopic) stress, σ_m is the mean (macroscopic) stress, $\overline{\sigma}$ is the current flow stress of the cell matrix material and f defines the current void fraction. Under multiaxial stress states, $\sigma_e = (3S_{ij}S_{ij}/2)^{1/2}$ where S_{ij} denotes the deviatoric components of Cauchy stress. Factors q_1, q_2 and q_3 introduced by Tvergaard improve the model predictions for periodic arrays of cylindrical and spherical voids; here we use $q_1 = 1.25$, $q_2 = 1.0$ and $q_3 = q_1^2$.

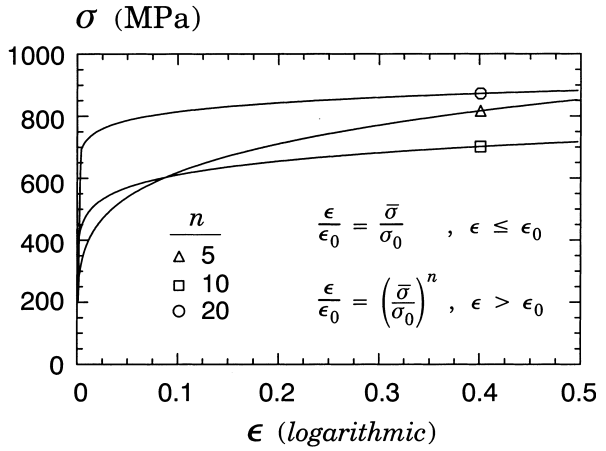

Fig. 5. Uniaxial true stress–logarithmic strain response of materials employed in the analyses using a power-hardening model.

The background material outside of the computational cells follows a J_2 flow theory with the Mises plastic potential obtained by setting $f \equiv 0$ in Eq. (9). The uniaxial true stress-logarithmic strain response for both the background and cell matrix materials follows a simple power-hardening model

$$\begin{aligned} \frac{\epsilon}{\epsilon_0} &= \frac{\overline{\sigma}}{\sigma_0}, \quad \epsilon \leqslant \epsilon_0; \\ \frac{\epsilon}{\epsilon_0} &= \left(\frac{\overline{\sigma}}{\sigma_0}\right)^n, \quad \epsilon > \epsilon_0, \end{aligned} \tag{10}$$

where σ_0 and ϵ_0 are the reference (yield) stress and strain, and n is the strain hardening exponent. Sections 4 and 5 describe numerical solutions for the SSY boundary-layer model with non-zero T-stress using materials with $n = 5$ (high hardening) with $E/\sigma_0 = 800$, $n = 10$ (moderate hardening) with $E/\sigma_0 = 500$ and $n = 20$ (low hardening) with $E/\sigma_0 = 300$; each with $\nu = 0.3$. The stress–strain response for these materials is shown in Fig. 5. These properties characterize a relatively wide range of plastic behavior for structural steels while, at the same time, reflecting the upward trend in yield stress with the decrease in strain hardening exponent characteristic of ferritic steels.

3.4. Finite element procedures

Finite element solutions are generated using the research code WARP3D (Koppenhoefer et al., 1994). Key features of the code employed in this work include: (1) the GT and Mises constitutive models implemented in a finite–strain setting, (2) cell extinction using a traction–separation model, (3) automatic load step siźing based on the rate of damage accumulation, and (4) evaluation of the J-integral using a domain integral procedure. Fructure models are constructed with 3-D, 8-node hexahedral elements. Use of the so-called $\overline{B}$ formulation (Hughes, 1980) precludes mesh lock-ups that arise as the deformation progresses into fully plastic, incompressible modes.

The local value of the mechanical energy release rate at a point along a crack front is given by Moran and Shih (1987)

$$J = \lim_{\Gamma \to 0} \int_{\Gamma} \left[\mathscr{W} n_1 - P_{ji} \frac{\partial u_i}{\partial X_1} n_j \right] \mathrm{d}\Gamma, \tag{11}$$

where Γ denotes a contour defined in a plane normal to the front on the undeformed configuration ($t = 0$) beginning at the bottom crack face and ending on the top face, n_j is the outward normal to Γ, $\mathscr{W}$ denotes the stress–work density per unit of undeformed volume, P_{ij} and u_i are Cartesian components of (unsymmetric) Piola–Kirchoff stress and displacement in the crack front coordinate system. Our finite element computations employ a domain integral procedure (Moran and Shih, 1987) for numerical evaluation of Eq. (11). A thickness average value for J is computed over domains defined outside material having the highly non-proportional histories of the near-tip fields and thus retains a strong domain (path) independence. Such J-values provide a convenient parameter to characterize the average intensity of far field loading on the crack front.

4. Measure of constraint using SSY fields

A convenient description for the diverse range of crack-tip fields (which depends on crack geometry and loading mode) can be motivated by considering the progression of plastic states under increased remote loading for a cracked body. At low loads, the near-tip stresses and deformations evolve according to a self-similar field characterized by a high level of stress triaxiality. As plastic flow progresses from well-contained yielding to LSY, the near-tip stresses gradually relax below the levels for high triaxiality stress states (see, for example, the early numerical analyses of McMeeking and Parks (1979), and Shih and German, 1981). This evolving level of stress triaxiality ahead of the crack front under increased remote loading is referred to as *constraint*.

The approach to quantify the level of constraint in a finite cracked body utilizes full "reference" crack-tip fields constructed for SSY conditions. The crack-tip fields computed for the finite body are then compared to SSY fields to define *relative* constraint differences. Finite element analyses of the MBL problem enable construction of SSY fields for general material response and admit the option to include finite–strain (blunting) effects at the crack tip. The plane–strain element mesh represents a single-ended crack in an infinite body where specified values for K_I and T uniquely define the linear-elastic remote field enclosing a vanishingly small plastic zone at the tip relative to other geometric dimensions such as crack size (see Fig. 4). Incremental plasticity theory, viscoplasticity and arbitrary material flow properties, for example, introduce no difficulties.

Fig. 6(a)–(d) provides key results to verify the existence of such fields for well-contained, limited scale plasticity under varying levels of applied T-stress for the material with $n = 10(E/\sigma_0 = 500)$. In the plots, distances all scale with $(K_I/\sigma_0)^2$ whereas the opening stresses are normalized by σ_0. At very low remote loading for all levels of applied T-stress ($K_I = 20, 40$ MPa $\sqrt{\text{m}}$), the near-tip stresses increase as the process of crack-tip blunting takes place. After the notch root radius increases to several times the initial radius ρ, a *steady state solution* develops so that the near-tip fields under SSY conditions are simply a continuous series of self-similar states. Additional results for analyses conducted for materials with $n = 5$ $(E/\sigma_0 = 800)$ and $n = 20$ $(E/\sigma_0 = 300)$ display essentially similar trends. Here, the crack-tip fields for these materials collapse onto a single normalized curve once sufficient crack-tip blunting occurs.

These plane–strain fields thus define a family of reference fields for stationary cracks where specified values for K_I and T uniquely define the elastic–plastic fields along the crack tip when a vanishingly small plastic zone encloses the tip. The differences between the actual finite–body field and those of the comparison SSY field (having the applicable elastic T-stress), quantify the extent of LSY effects. Despite the *apparent* small differences between these fields (differences between high and low constraint fields are of the order of $\sim$10%), the implications for fracture are enormous as demonstrated by experimental observations. Indeed, factors exceeding 3–5 are often observed in toughness values K_{Ic}, J_c or δ_c for high constraint and low constraint fracture specimens. This aspect will become more evident in Section 5.

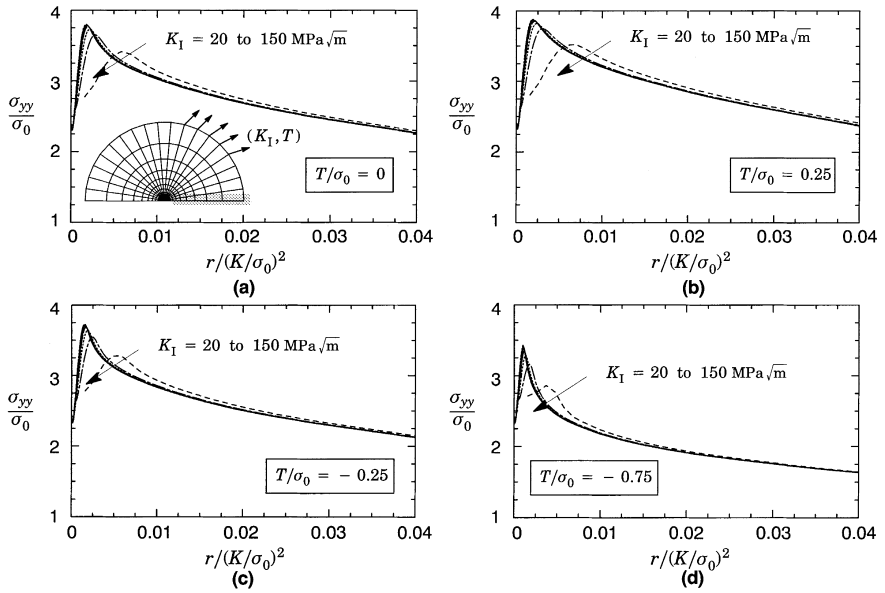

Fig. 6. Near-tip opening stresses under SSY conditions for $n = 10$, $E/\sigma_0 = 500$ and varying levels of applied T-series. Plots are generated for load levels $K_I = 20$, 40, 60, 80, 100, 125 and 150 MPa $\sqrt{m}$.

In the present context pertaining to a local approach to cleavage fracture, the SSY reference solutions provide the necessary fields to compute the evolution of the Weibull stress with K_I and T as well as ductile tearing. For a fixed set of material dependent constants in the microscale fracture criterion, these relationships constitute the SSY reference conditions to assess the strong effects of constraint and stable crack growth on fracture resistance.

5. Constraint and ductile tearing effects on fracture

This section provides key results for the SSY analyses under varying levels of T-stress used to assess effects of crack-tip constraint and ductile tearing on fracture resistance. The presentation begins with descriptions for the evolution of Weibull stress with crack-tip stress triaxiality and then turns to effects of crack growth on Weibull stress trajectories. A central feature of the present investigation involves the interpretation of σ_w as a *macroscopic* crack driving force and the implications of its use in assessments of brittle fracture behavior. For convenience, the plane–strain SSY analyses utilize finite element models with a *reference* unit thickness, $B = 1$ mm, throughout.

5.1. The Weibull stress for stationary cracks

SSY solutions with varying levels of applied T-stress are generated for power–law hardening materials having three levels of strain hardening: $n = 5$ $(E/\sigma_0 = 300)$, $n = 10$ $(E/\sigma_0 = 500)$ and $n = 20$ $(E/\sigma_0 = 800)$. In each analysis, the full value of T-stress is imposed first (which causes no yielding), followed by the K_I field imposed in an incremental manner. In evaluating the Weibull stress, Eq. (3), under increasing K_I levels, the value of the Weibull modulus is adopted as $m = 10$ for the high strain hardening material $(n = 5)$ and $m = 20$ for the moderate to low-hardening material $(n = 10$ and $20)$. In particular, values for $m \approx 20$

characterize the distribution of Weibull stress at cleavage fracture for a nuclear pressure vessel steel (ASTM A508) (Beremin, 1983). For the analyses of the moderate strain hardening material ($n = 10$) with $T/\sigma_0 = 0$, two other values of the Weibull modulus are also considered: $m = 10$ and 30. This range of parameter covers most m-values for structural steels reported by Gao et al. (1998) and Ruggieri et al. (in press).

Fig. 7(a)–(c) shows the variation of Weibull stress under increasing deformation for the three levels of hardening $n = 5$, 10, 20 and for values of T-stress ranging from $-0.75 \leqslant T/\sigma_0 \leqslant 0.5$. The T-stress values adopted in our analyses are consistent with the ranges defined by SSY analyses (see, e.g., Parks, 1992). For $T/\sigma_0 = 0$ and fixed strain hardening ($n = 10$), Fig. 7(d) shows the variation of Weibull stress with increasing deformation for $m = 10$, 20 and 30. In these plots, $K_I^2/(\sigma_0^2 R)$ describes the far-field loading with the Weibull stress normalized by the yield stress, σ_0. For each material, the evolution of σ_w as deformation progresses depends markedly on the level of crack-tip stress triaxiality as measured by T/σ_0. The Weibull stress trajectories for positive values of T/σ_0 are consistently above the corresponding trajectories for $T/\sigma_0 = 0$. Conversely, the evolutions of σ_w for negative values of T/σ_0 remain below the Weibull stress curve for $T/\sigma_0 = 0$. Since the Weibull stress and the far-field loading in each plot are normalized by the material's yield stress, σ_0, direct comparison of the fracture resistance behavior for the materials is somewhat difficult. However, these results demonstrate clearly the strong effect of constraint loss ($T/\sigma_0 < 0$) on the levels of σ_w for all materials, particularly for moderate to low hardening materials ($n = 10$–20). The effects of T/σ_0 on σ_w observed here are entirely consistent with the J–Q characterization of SSY stress fields described by O'Dowd and Shih (1991, 1992). The lower σ_w-values with $T/\sigma_0 < 0$ follow from the reduced stress triaxiality levels ahead of the crack tip, as described by negative Q-values.

A central feature of the above results is that the failure probability for the stressed cracked body at fixed values of T/σ_0 monotonically increases for increased σ_w-values. This conclusion derives directly from the coupling between the Weibull stress and loading as implied by Eq. (3) in conjunction with Eq. (4). The results displayed by these plots also support observations about the strong effect of small differences in near-tip stresses for high and low constraint configurations on cleavage fracture behavior made previously.

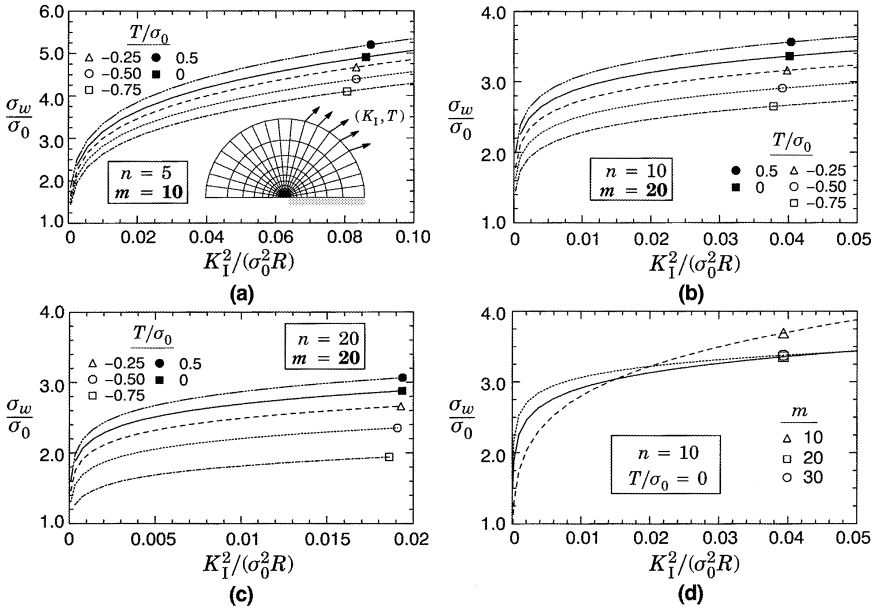

Fig. 7. Stationary crack analysis under SSY conditions and varying hardening properties.

In other words, larger K-values in the finite body are necessary to increase the crack-tip driving force, as expressed by σ_w in Fig. 7, such as local conditions to trigger cleavage fracture can be reached. This conclusion applies for other loading measures such as J and CTOD.

Another important feature of these results is the similar shape of σ_w-trajectories with T/σ_0 after the early stages of loading; here, the magnitude of Weibull stress all scale with T/σ_0 in accordance with $\sigma_w = \beta_m K_I^{4/m}$ (Mudry, 1987), where the proportionality constant, β_m, depends on m as exhibited by the plots displayed in Fig. 7(d). Because parameter T/σ_0 scales the near-tip stresses relative to the reference field ($T/\sigma_0 = 0$), as presented in Fig. 6, it also affects the magnitude of the Weibull stress at rates that decrease (increase) with reduced (increased) stress triaxiality. Consequently, the evolution of Weibull stress with remote loading can be generalized as $\sigma_w = \beta_{T,m} K_I^{4/m}$, where the proportionality constant, $\beta_{T,m}$, depends on m and T/σ_0.

5.2. Effects of ductile tearing on the Weibull stress

The SSY analyses for a growing crack provides the basis to extend the Weibull stress as a broadly applicable fracture parameter for cleavage failure. This section examines the effects of ductile tearing on the Weibull stress and implications on fracture behavior of cracked bodies that exhibit small amounts of stable crack growth before cleavage failure. To conserve space, we describe only key results computed for the $n = 10$ material with $f_0 = 0.001$; similar trends and conclusions remain valid for other f_0 values.

Fig. 8(a) shows the computed crack growth resistance curves for this set of material properties. J is normalized by the cell size and flow stress ($D\sigma_0$) while Δa is normalized by D. The cell with current porosity $f = 0.1$ defines the current crack-tip location, and thus Δa. This "operational" definition locates the crack-tip in the region behind the peak stress where stresses decrease rapidly, but ahead of the very highly damaged region, where the GT model does not accurately predict material response. Fig. 8(a)–(d) present the dependency of σ_w, Eq. (5), on crack growth for three values of the shape parameter: $m = 10$, 20 and 30. For all levels of crack-tip constraint represented by T/σ_0, the Weibull stress increases monotonically with ductile extension. While the *apparent* rate at which σ_w increases is smaller than the behavior displayed in

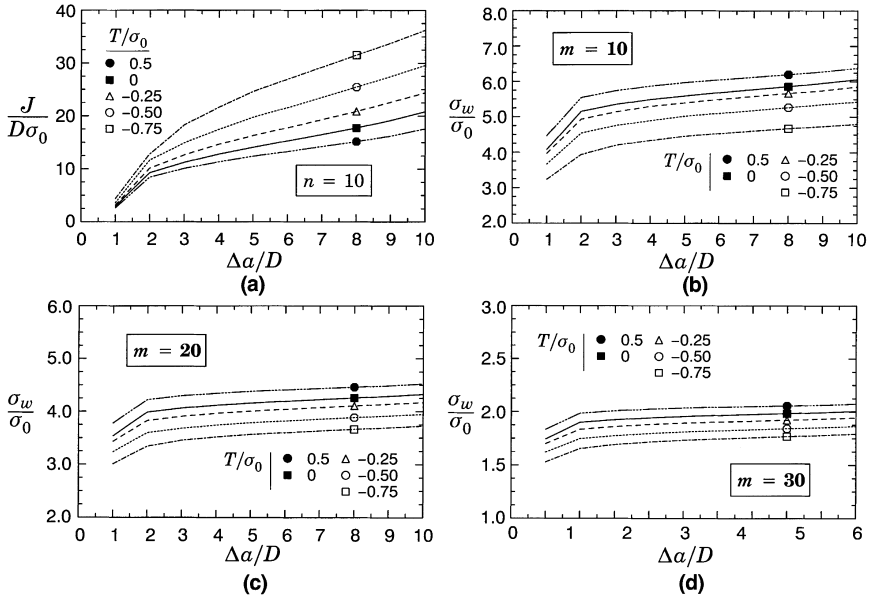

Fig. 8. Crack growth analyses under SSY conditions for $n = 10$ ($E/\sigma_0 = 500$) and $f_0 = 0.001$ with varying values of parameter m.

Fig. 7, it must be emphasized that σ_w is plotted against crack growth Δa and *not* against the loading parameter J. In the present context, such results clearly demonstrate that small amounts of stable crack growth do increase the propensity for cleavage fracture as measured by σ_w. Another interesting feature is that smaller values of the shape parameter m have greater impact on σ_w vs. Δa trajectories, i.e., $d\sigma_w/da$ increases with decreased m. However, this effect is less pronounced when m varies from 30 to 20.

Additional results for materials having $n = 5$ and 20 with $f_0 = 0.001$ are presented in Fig. 9(a)–(d) for Weibull moduli of $m = 10$ and 20. The trends observed for the material with $n = 10$ persist for the materials analyzed here. However, σ_w-values for the high hardening material exhibits a weak dependence on ductile tearing for all values of T/σ_0, particularly for negative T-stress. Additional insight into this behavior can be gained by considering the corresponding R-curves for this material. For negative values of T/σ_0, essentially steady-growth conditions ($dJ/da \to 0$) develop after only a few cells of crack extension. Such behavior characterizes a ductile tearing mechanism ahead of the crack tip with essentially constant peak opening stress. Indeed, the analyses by Xia and Shih (1995a) convincingly demonstrate that crack growth under steady conditions exhibit a constant peak stress value during further growth and an essentially fixed distance between the peak stress location and the crack tip. Because the Weibull stress reflects a stress integral over material points well ahead of the advancing crack tip and, further, the high values for parameter m magnifies the impact of variations in the near-tip stress fields, the levels of σ_w are relatively unchanged as crack growth progresses.

These representative analyses aid in understanding the effects of stable crack growth on the propensity of brittle fracture for a cracked body. Consider first the results for a stationary crack presented in Fig. 7. As previously noted, increasing Weibull stress values with increased loading imply increased failure probability for the cracked body. Examination of Eq. (5) reveals that such behavior arises from either: (a) increased FPZ size (i.e., increased volume Ω); (b) increased near-tip stresses. When a cracked body loses constraint, the near-tip stresses relax below the values for the high constraint configuration. Consequently, σ_w-values also fall below SSY values and fracture cannot take place unless some other mechanism occurs. Consider

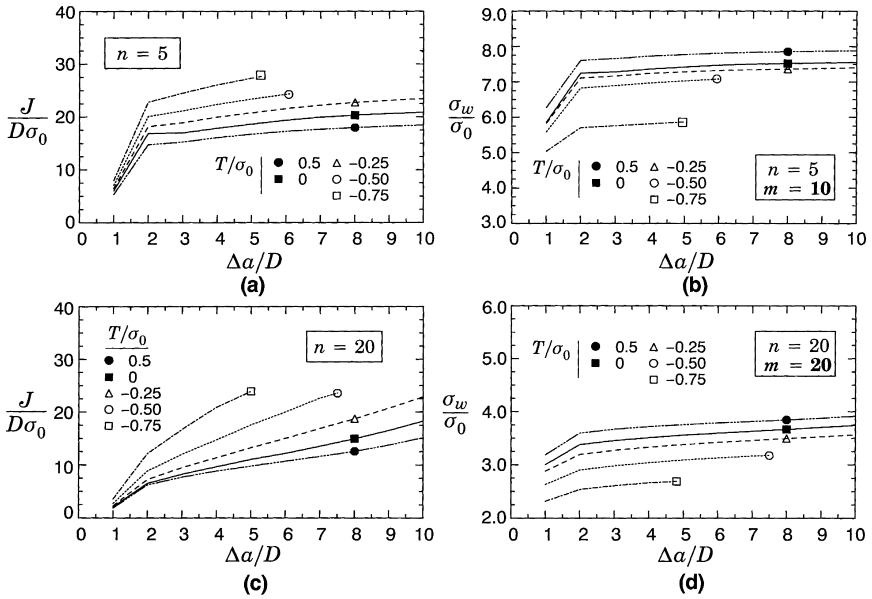

Fig. 9. Crack growth analyses under SSY conditions for $n = 5$ ($E/\sigma_0 = 800$) and $n = 20$ ($E/\sigma_0 = 300$) with $f_0 = 0.001$ and varying values of parameter m.

now a cracked body that has experienced loss of constraint but which still fails by cleavage mode. Such behavior is most often observed when testing structural steels at certain temperatures within the transition region (particularly in mid transition region) where brittle fracture is frequently accompanied by small amounts of ductile tearing. Following the intense near-tip blunting process for the stationary crack (where the stresses relax significantly), ductile tearing has the effect of "recovering" (at least partly) the high constraint conditions at the crack tip. The trends shown here are consistent with those obtained in previous numerical analyses (Varias and Shih, 1993; Dodds et al., 1993) in that stable crack growth elevates the near-tip stresses and increases the volume of the cleavage FPZ. Based upon the notion of σ_w as the *crack-tip driving force*, these results demonstrate that low constraint configurations must undergo further loading (as measured by J), often accompanied by ductile tearing, to reach a critical value of the Weibull stress, $\sigma_{w,c}$, that triggers cleavage fracture.

6. Assessment of constraint effects in a fracture specimen

This section outlines a toughness scaling methodology based upon the Weibull stress to assess effects of constraint loss in conventional fracture specimens. The numerical results for the SSY model and 3-D finite element analyses of the standard SE(B) specimens with size 1(T) are employed to *correlate* constraint loss on individual fracture toughness values for different material properties ($J_{LSY} \rightarrow J_{SSY}$ trajectories). The objective is to support the applicability of the methodology to quantify the extent of LSY that develops in fracture specimens.

Fig. 10 illustrates the procedure to assess the effects of constraint loss on fracture toughness needed to construct (J_{LSY} vs. J_{SSY} trajectories. Very detailed, non-linear 3-D finite element analyses provide the functional relationship between the Weibull stress (σ_w) and the applied loading (J) for a specified value of the Weibull modulus, m. The research code *WSTRESS* (Ruggieri and Dodds, 1997) is employed to compute the Weibull stress for all analyses. Based upon the argument of the Weibull stress as the crack driving force, the scaling model requires the attainment of equal values for σ_w to trigger cleavage fracture across different specimen geometries even though J-values may vary widely due to constraint loss. Fig. 10 shows curves of σ_w vs. J for a standard fracture specimen (the present work employs only 1(T) deep notch SE(B) specimens) and for a plane–strain, SSY reference solution ($T/\sigma_0 = 0$) with the *same thickness of the fracture specimen*. Such curves are constructed for a fixed, representative value of the Weibull modulus, m, for each set of mechanical properties flow properties (the normalizing volume for the Weibull stress, V_0, is

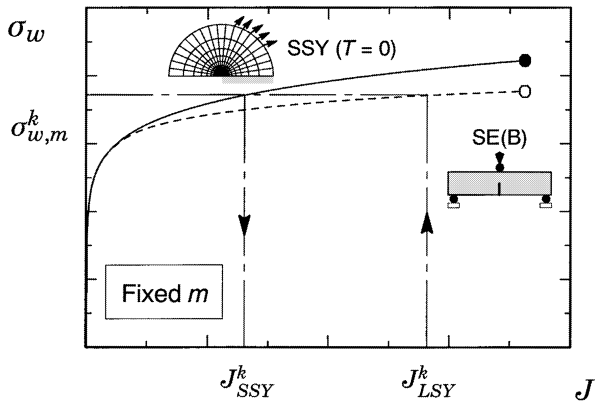

Fig. 10. Toughness scaling model used to construct $J_{LSY} \rightarrow J_{SSY}$ corrections.

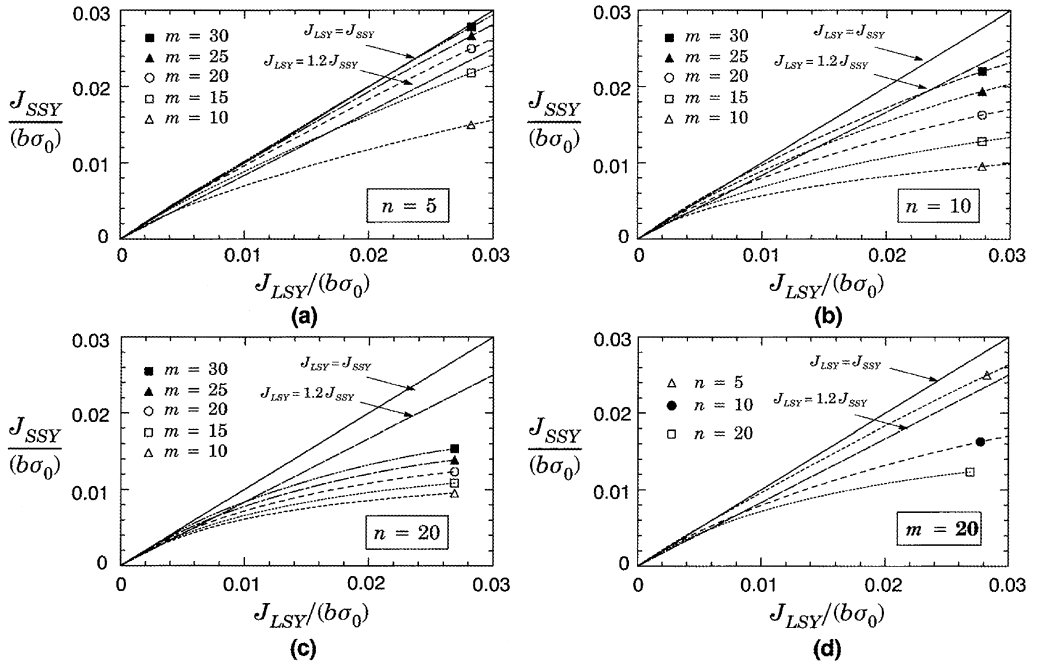

Fig. 11. $J_{LSY} \rightarrow J_{SSY}$ correction using a scaling methodology based upon the Weibull stress with varying Weibull moduli for plane-sided 1(T) SE(B) specimens. J-values are normalized by crack ligament, $b = W - a$, and yield stress σ_0.

conveniently assigned the value of 1 mm^3). J_{LSY} values computed from the domain integral procedures in the finite element analyses of the SE(B) specimens represent thickness average values, which are consistent with experimental (average) values. For the plane–strain SSY model, J_{SSY} becomes simply the J value at the crack tip. Even the J_{LSY} value for the fracture specimen, the lines shown on Fig. 10 readily illustrate the technique used to determine J_{SSY}.

Fig. 11(a)–(d) provides the constraint corrections (LSY $\rightarrow$ SSY) for the 1(T) SE(B) specimens with different material properties ($n = 5$ with $E/\sigma_0 = 800$; $n = 10$ with $E/\sigma_0 = 500$; $n = 20$ with $E/\sigma_0 = 300$) and for varying Weibull moduli, m. The present computations consider values of $m = 10$, 15, 20, 25 and 30 to assess the sensitivity of constraint corrections on the specified Weibull modulus. As noted before, these m-values are consistent with previously reported values for structural steels. Each curve provides pairs of J-values, J_{LSY} in the SE(B) specimen and J_{SSY} in SSY, that produce the same σ_w. Reference lines are shown which define a constant ratio of "constraint loss", e.g., $J_{avg} = 1.2 \times J_0$ which implies that the SE(B) average J must be 20% larger than the SSY value to generate the same Weibull stress. For each value of the Weibull modulus, the SE(B) and SSY curves agree very well early in the loading history while the SE(B) specimen maintains near SSY conditions across the crack front (recall that computation of σ_w in the SE(B) specimens considers the entire crack front). Once near-front stresses deviate from the (plane–strain) SSY levels, the σ_w curves for the SE(B) specimens fail to increase at the same rate with further loading. These results clearly illustrate the gradual nature of constraint loss in the deep-notch SE(B) specimens, especially for moderate to low hardening materials. The Weibull modulus does have an appreciable affect on predictions of constraint loss; increasing m values indicate a higher load level at the onset of constraint loss and a reduced rate of constraint loss under further loading. The larger m values, in effect, assign a greater weight factor to stresses at locations very near the crack front. The bending field, which impinges on the crack front, affects the smaller m curves more readily.

7. Concluding remarks

We have presented a computational framework for brittle fracture which incorporates weakest link statistics and a micromechanics model reflecting local damage of the material. The approach addresses the strong effects of constraint variations on (macroscopic) cleavage fracture toughness which also includes modeling of ductile tearing when cleavage failure is preceded by small amounts of stable crack growth. The Weibull stress (σ_w) emerges as a probabilistic fracture parameter to define conditions leading to (local) material failure. Unstable crack propagation occurs at a critical value of σ_w which may be attained prior to or following some amount of stable, ductile crack extension. When implemented in a finite element code, the computational model predicts the evolution of Weibull stress with applied load (conveniently measured by J in the present work) while the crack tip undergoes first blunting and then stable, ductile crack extension. The SSY analyses under varying levels of T-stress presented in our study provide valuable insight about the effects of crack-tip constraint on fracture resistance. These SSY results exhibit the essential features of the micromechanics approach in correlating macroscopic fracture toughness with constraint variations and ductile tearing. Application of the methodology in the form of a toughness scaling model provides a simple procedure to *correct* toughness values for effects of constraint loss in conventional fracture specimens.

However, because the model also simplifies a seemingly complex array of metallurgical processes and operative mechanisms at the microlevel, the application of the model in fracture mechanics applications, particularly in fracture assessments procedures (i.e., predictions of fracture events in large engineering structures), still remains untested. In particular, robust schemes to calibrate the Weibull parameters (m, σ_u) become a key element to correlate effects of constraint loss for varying crack configurations and loading modes (tension vs. bending) based upon σ_w. Preliminary efforts along these lines have recently been made by Gao et al., (1998) who introduced a new, improved calibration procedure for the Weibull parameters (m, σ_u). Ongoing work is currently underway to extend the model into a full 3-D framework to correlate through-crack fracture specimens and surface-crack components.

Acknowledgements

This investigation was supported by grants principally from the Scientific foundation of the State of São Paulo (FAPESP) under Grant 98/10574-2. Computational support provided by the High Performance Computing Center (LCCA) of the University of São Paulo is also acknowledged.

References

Beremin, F.M., 1983. A local criterion for cleavage fracture of a nuclear pressure vessel steel. Metallurgical Transactions 14A, 2277–2287.

De Castro, P.M.S.T., Spurrire, J., Hancock, P., 1979. An experimental study of the crack length/specimen width (a/W) ratio dependence of the crack opening displacement (COD) test using small-scale specimens. In: Smith, C.W. (Ed.), Fracture Mechanics, ASTM STP 677, American Society for Testing and Materials, Philadelphia, Pennsylvania, pp. 486–497.

Dodds, R.H., Tang, M., Anderson, T.L., 1993. Numerical modeling of ductile tearing effects on cleavage fracture toughness. In: Kirk, M., Bakker, A. (Eds.), Constraint Effects in Fracture, Theory and Application. ASTM STP 1244, American Society for Testing and Materials, Philadelphia, Pennsylvania.

Evans, A.G., Langdon, T.G., 1976. Structural ceramics. In: Chalmers, B. (Ed.), Progress in Materials Science. Vol. 21, Pergamon Press, NY, pp. 171–441.

Feller, W., 1957. Introduction to Probability Theory and its Application. Vol. 1, Wiley, New York.

Freudenthal, A.M., 1968. Statistical approach to brittle fracture. In: Liebowitz, H. (Ed.), Fracture: An Advanced Treatise. Volume II, Academic Press, NY, pp. 592–619.

Gao, X., Ruggieri, C., Dodds, R.H., 1998. Calibration of Weibull stress parameters using fracture toughness data. International Journal of Fracture 92, 175–200.

Gurson, A.L., 1977. Continuum theory of ductile rupture by void nucleation and growth: Part I – Yield criteria and flow rules for porous ductile media. Journal of Engineering Materials and Technology 99, 2–15.

Hughes, T.J., 1980. Generalization of selective integration procedures to anisotropic and nonlinear media. International Journal for Numerical Methods in Engineering 15, 1413–1418.

Hutchinson, J.W., 1983. Fundamentals of the phenomenological theory of nonlinear fracture mechanics. Journal of Applied Mechanics 50, 1042–1051.

Koppenhoefer, K., Gullerud, A., Ruggieri, C., Dodds, R., Healy, B., 1994. WARP3D: dynamic nonlinear analysis of solids using a preconditioned conjugate gradient software architecture. Structural Research Series (SRS) 596, UILU-ENG-94-2017, University of Illinois at Urbana, Champaign.

Larsson, S.G., Carlsson, A.J., 1973. Influence of non-singular stress terms and specimen geometry on small scale yielding at crack-tips in elastic–plastic materials. Journal of the Mechanics and Physics of Solids 21, 447–473.

McMeeking, R.M., Parks, D.M., 1979. On criteria for *J*-dominance of crack-tip fields in large-scale yielding. In: Landes, J.D., Begley, J.A., Clark, G.A. (Eds.), Elastic–Plastic Fracture, ASTM STP 668, American Society for Testing and Materials, Philadelphia, Pennsylvania, pp. 175–194.

Moran, B., Shih, C.F., 1987. A general treatment of crack tip contour integrals. International Journal of Fracture 35, 295–310.

Mudry, F., 1987. A local approach to cleavage fracture. Nuclear Engineering and Design 105, 65–76.

O'Dowd, N.P., Shih, C.F., 1991. Family of crack-tip fields characterized by a triaxiality parameter: Part I – Structure of fields. Journal of the Mechanics and Physics of Solids 39 (8), 989–1015.

O'Dowd, N.P., Shih, C.F., 1992. Family of crack-tip fields characterized by a triaxiality parameter: Part II – Fracture applications. Journal of the Mechanics and Physics of Solids 40, 939–963.

Parks, D.M., 1992. Advances in characterization of elastic–plastic crack-tip fields. In: Argon, A.S. (Ed.), Topics in Fracture and Fatigue. Springer, pp. 59–98.

Rice, J.R., 1974. Limitations to the Small scale yielding approximation for crack tip plasticity. Journal of the Mechanics and Physics of Solids 22, 17–26.

Ruggieri, C., Dodds, R.H., 1996a. A transferability model for brittle fracture including constraint and ductile tearing effects: a probabilistic approach. International Journal of Fracture 79, 309–340.

Ruggieri, C., Dodds, R.H., 1996b. Probabilistic modeling of brittle fracture including 3-D effects on constraint loss and ductile tearing. Journal de Physique 6, 353–362.

Ruggieri, C., Dodds, R.H., 1996c. Numerical modeling of ductile crack growth in using computational cell elements. International Journal of Fracture 82, 67–95.

Ruggieri, C., Dodds, R.H., 1997. WSTRESS release 1.0: numerical computation of probabilistic fracture parameters for 3-D cracked solids. BT-PNV-30 (Technical Report), EPUSP, University of São Paulo.

Ruggieri, C., Dodds, R.H., 1998. Numerical computation of probabilistic fracture parameters using WSTRESS. Engineering Computations 15, 49–73.

Ruggieri, C., Gao, X., Dodds, R.H., inpress. Transferability of elastic–plastic fracture toughness using the Weibull stress approach: significance of parameter calibration. Engineering Fracture Mechanics.

Shih, C.F., German, M.D., 1981. Requirements for a one parameter characterization of crack tip fields by the HRR singularity. International Journal of Fracture 17 (1), 27–43.

Sorem, W.A., Dodds, R.H., Rolfe, S.T., 1991. Effects of crack depth on elastic plastic fracture toughness. International Journal of Fracture 47, 105–126.

Tvergaard, V., 1990. Material failure by void growth to coalescence. Advances in Applied Mechanics 27, 83–151.

Varias, A.G., Shih, C.F., 1993. Quase-static crack advance under a range of constraints – steady state fields based on a characteristic length. Journal of the Mechanics and Physics of Solids 41, 835–861.

Weibull, W., 1939. The phenomenon of rupture in solids. Ingeniors Vetenskaps Akademien, Handlingar, vol. 153, p. 55.

Williams, M.L., 1957. On the stress distribution at the base of a stationary crack. Journal of Applied Mechanics 24, 109–114.

Xia, L., Shih, C.F., 1995a. Ductile crack growth – I. A numerical study using computational cells with microstructurally-based length scales. Journal of the Mechanics and Physics of Solids 43, 233–259.

Xia, L., Shih, C.F., Hutchinson, J.W., 1995b. A computational approach to ductile crack growth under large scale yielding conditions. Journal of the Mechanics and Physics of Solids 43, 398.